An anaplerotic approach to correct the mitochondrial dysfunction in ataxia-telangiectasia (A-T)

Original Article

MOLECULAR METABOLISM

An anaplerotic approach to correct the mitochondrial dysfunction in ataxia-telangiectasia (A-T)

A.J. Yeo [1,**], G.N. Subramanian [1], K.L. Chong [1], M. Gatei [1], R.G. Parton [2], D. Coman [3,4], M.F. Lavin [1,*]

ABSTRACT

Background: ATM, the protein defective in the human genetic disorder, ataxia-telangiectasia (A-T) plays a central role in response to DNA double-strand breaks (DSBs) and in protecting the cell against oxidative stress. We showed that A-T cells are hypersensitive to metabolic stress which can be accounted for by a failure to exhibit efficient endoplasmic reticulum (ER)-mitochondrial signalling and $Ca2^{+}$ transfer in response to nutrient deprivation resulting in mitochondrial dysfunction. The objective of the current study is to use an anaplerotic approach using the fatty acid, heptanoate (C7), a metabolic product of the triglyceride, triheptanoin to correct the defect in ER-mitochondrial signalling and enhance cell survival of A-T cells in response to metabolic stress.

Methods: We treated control cells and A-T cells with the anaplerotic agent, heptanoate to determine their sensitivity to metabolic stress induced by inhibition of glycolysis with 2- deoxyglucose (2DG) using live-cell imaging to monitor cell survival for 72 h using the Incucyte system. We examined ER-mitochondrial signalling in A-T cells exposed to metabolic stress using a suite of techniques including immunofluorescence staining of Grp75, ER-mitochondrial Ca^{2+} channel, the VAPB-PTPIP51 ER-mitochondrial tether complexes as well as proximity ligation assays between Grp75-IP3R1 and VAPB1-PTPIP51 to establish a functional interaction between ER and mitochondria. Finally, we also performed metabolomic analysis using LC-MS/MS assay to determine altered levels of TCA intermediates A-T cells compared to healthy control cells.

Results: We demonstrate that heptanoate corrects all aspects of the defective ER-mitochondrial signalling observed in A-T cells. Heptanoate enhances ER-mitochondrial contacts; increases the flow of calcium from the ER to the mitochondrion; restores normal mitochondrial function and mitophagy and increases the resistance of ATM-deficient cells and cells from A-T patients to metabolic stress-induced killing. The defect in mitochondrial function in ATM-deficient cells was accompanied by more reliance on aerobic glycolysis as shown by increased lactate dehydrogenase A (LDHA), accumulation of lactate, and reduced levels of both acetyl CoA and ATP which are all restored by heptanoate.

Conclusions: We conclude that heptanoate corrects metabolic stress in A-T cells by restoring ER-mitochondria signalling and mitochondrial function and suggest that the parent compound, triheptanoin, has immense potential as a novel therapeutic agent for patients with A-T.

Keywords Ataxia-telangiectasia; ATM; Nutrient deprivation; Endoplasmic reticulum—mitochondrial interaction; Mitochondrial dysfunction; Heptanoate (C7)

1. INTRODUCTION

The multisystem disorder, ataxia-telangiectasia (A-T, OMIM Entry: #208900), is characterized by neurodegeneration, immunodeficiency, recurrent pulmonary infections, increased risk of diabetes, liver disease, oxidative stress, increased sensitivity to ionizing radiation, and susceptibility to cancer [1,2]. ATM serine/threonine kinase (ATM), the protein defective in A-T, is activated by DNA double-strand breaks (DSBs) by recruitment to the sites of damage by the MRE11/RAD50/NBS1 (MRN) complex [3,4]. Activation is achieved by post-translational modifications including auto-phosphorylation at several sites and the conversion of an inactive dimer to an active monomer [5–7]. Once activated, ATM phosphorylates all three members of the MRN complex, which act as mediators for the phosphorylation of a multitude of substrates involved in cell cycle control, DNA repair, and other cellular processes [1,8].

Treatment of cells with histone deacetylase inhibitors, hypotonic conditions, chloroquine, and mitochondrial electron transport inhibitors also activate ATM by a mechanism involving auto-phosphorylation but not involving DNA damage [5,9]. ATM is activated by Reactive oxidative species (ROS) by a distinct mechanism involving disulphide bond

[1]University of Queensland Centre for Clinical Research, University of Queensland, Herston, Brisbane, Australia [2]Institute for Molecular Bioscience and Centre for Microscopy and Microanalysis, University of Queensland, St Lucia, Brisbane, Australia [3]Queensland Children's Hospital, Brisbane, Australia [4]Faculty of Medicine, University of Queensland, Herston, Brisbane, Australia

*Corresponding author. Level 6, UQCCR, 71/918 Royal Brisbane and Women's Hospital Campus, Herston, Queensland 4029, Australia. E-mail: m.lavin@uq.edu.au (M.F. Lavin).

**Corresponding author. Level 6, UQCCR, 71/918 Royal Brisbane and Women's Hospital Campus, Herston, Queensland 4029, Australia. E-mail: abrey.yeo@uq.edu.au (A.J. Yeo).

Received July 1, 2021 • Revision received September 22, 2021 • Accepted October 6, 2021 • Available online 9 October 2021

https://doi.org/10.1016/j.molmet.2021.101354

formation between two ATM monomers without the requirement for the MRN complex [10]. Separation-of-function mutants have shown demonstrating two ATM activation pathways driven by DNA DSBs and oxidative damage, respectively [11]. Activation induced by oxidative stress does not lead to phosphorylation of DNA damage effectors such as H2AX and KAP1 [11]. A functional role for ATM in combating oxidative stress is supported by hypersensitivity to ROS in A-T cells [12,13]; generation of oxidative stress in the absence of ATM [14], and protection of ATM-deficient cells and mice by antioxidants [15–17]. The association of ATM with both mitochondria [9,18] and peroxisomes [19,20] fits well with a model where ATM is a sensor of oxidative stress [21]. Though some controversy exists concerning the exact nature of mitochondrial abnormalities in A-T, most findings agree that mitochondrial homeostasis is dysregulated in the absence of ATM signalling. Ambrose et al. [22] reported reduced mitochondrial mass in lymphoblastoid cells but the number of mitochondria showed similarity in A-T and control cells. Reduced mitochondrial mass was also reported for A-T fibroblasts which were more pronounced after irradiation but was attributed to an imbalance between mitochondrial DNA copy number and mitochondrial biogenesis [23]. In contrast, several recent reports provide evidence for increased mitochondrial mass in A-T cells and in $Atm^{-/-}$ thymocytes [9,24–26]. This is supported by a defect in mitophagy in A-T cells.

We recently showed that ATM is also activated by inhibition of glycolysis by a mechanism that does not appear to involve DNA damage and that ATM-deficient cells are exquisitely sensitive to DNA damage-related metabolic stress [26]. We demonstrated that endoplasmic reticulum (ER)-mitochondrial connectivity through the voltage-dependent calcium channel (VDAC1) and the inositol 1,4,5 triphosphate receptor type 1 (IP3R1), mediated by the mitochondrial chaperone Grp75, is defective in A-T cells after nutrient stress. This signalling defect led to a deficiency in maintaining calcium homeostasis, which can account for at least part of the mitochondrial dysfunction in A-T cells. These results suggest that when glycolysis is inhibited the capacity of mitochondria to compensate for energy deficiency in ATM-deficient cells is limited and it could be accounted for by reduced TCA cycle activity [25,26]. Triheptanoin, a triglyceride of the three odd-chain fatty acids (heptanoate, C7), has been applied for the treatment of several neurological diseases and those due to disturbed glucose metabolism, in which the energy supply from citric acid cycle intermediates or fatty acid degradation is impaired [27]. It recently received its first regulatory approval for use in the US as a source of calories and fatty acids for the treatment of paediatric and adult patients with molecularly confirmed long-chain fatty acid oxidation disorders [28]. Triheptanoin functions as an anaplerotic agent replenishing tricarboxylic acid (TCA) cycle intermediates by metabolism to heptanoate (C7) and subsequently acetyl-CoA and propionyl-CoA that feed into the TCA cycle to supply energy [29]. This compound has been shown to mitigate brain ATP depletion and mitochondrial dysfunction, including respiration and redox balance in a mouse model of Alzheimer's disease, supporting the energy failure hypothesis for that disorder [30]. We describe here the correction of ER-mitochondrial signalling and mitochondrial function in ATM-deficient cells using heptanoate, a metabolite of triheptanoin [27]. This approach has the potential for a novel therapy for patients with A-T.

2. METHODS AND MATERIALS

2.1. Cell culture

HBEC3-KT and ATM-deficient HBEC3-KT cells (B3) were cultivated in Keratinocyte-SFM (KSFM) (Ref. 10,724,011; Thermo Fisher Scientific, MA, USA) supplemented with 100 U/ml penicillin/streptomycin (Thermo Fisher Scientific, MA, USA). The cultures were maintained in a humidified incubator at 37 °C with 5% CO_2.

Olfactory neurosphere (ONS)-derived cells were established as described previously [76]. Briefly, following nasal biopsy from healthy controls, primary cells from A-T patients were grown in Dulbecco's Modified Eagle's Medium/Ham F-12 (DMEM/F12; Ref. 11,320,033; Thermo Fisher Scientific, MA, USA) containing 10% foetal bovine serum (FBS; Ref. 10,437,028; Thermo Fisher Scientific, MA, USA) and 1% streptomycin/penicillin (Ref. 15,240,122; Thermo Fisher Scientific, MA, USA). While performing the cell survival assay in the Incucyte S3, the ONS cells were grown in DMEM (Ref. 11,885,084; Thermo Fisher Scientific, MA, USA) supplemented with 5 mM Glucose (Ref. A2494001; Thermo Fisher Scientific, MA, USA)

2.2. Sensitivity to 2DG and rescue with C7

Cells were treated with 15 mM 2-deoxyglucose (D6134, Sigma Aldrich, MA, USA), 750 μM heptanoate (C7; 75190; Sigma Aldrich, MA, USA). Cell death over a minimum of 72 h was determined using the Nuc-Green Dead 488 ReadyProbes Reagent (Thermo Fisher Scientific, MA, USA) as per the manufacture's protocol and observed using the IncuCyte S3 (Essen BioScience Inc., MI, USA).

2.3. Immunoblotting and immunofluorescence

Immunoblotting and immunofluorescence were performed as described in [26]. Primary antibodies used at 1:1000 (immunoblotting) and 1:100 (immunofluorescence) are as follows: anti-ATM (5C2) (GTX70107; Genetex, CA, USA), anti-ATM phospho-Ser1981 (ab81292; Abcam, Cambridge, U.K), anti-Grp75 (ab2799; Abcam, Cambridge, U.K), anti-VDAC1 (ab15895; Abcam, Cambridge, U.K), anti-IP3R1 (ab5804; Abcam, Cambridge, U.K), anti-VAPB (736,904, R&D Systems, MN, USA) and anti- PTPIP51 (NBP184738, CO, USA). Secondary antibodies used for immunofluorescences at 1:250 dilution are as follows: Alexa Fluor 594 goat anti-mouse (A-11032; Thermo Fisher Scientific, MA, USA) and Alexa Fluor 488 chicken anti-rabbit (A-24114; Thermo Fisher Scientific, MA, USA). Secondary antibodies used for immunoblotting at 1:5000 dilution are as follows: HRP-conjugated donkey anti-mouse (AP192P; Merck Millipore, MA, USA) and HRP-conjugated donkey anti-rabbit (AP182P; Merck Millipore, MA, USA).

2.4. Electron microscopy

Cells in 3 cm diameter plastic dishes were cultured as mentioned above, with and without incubation with 2DG. The cells were fixed using 2.5% glutaraldehyde in PBS (pH 7.4) for 1 h at RT and then washed 3x with PBS. The fixed cells were then stained with 3% potassium ferricyanide and 2% osmium tetroxide in 0.1 M cacodylate buffer for 30 min, then x3 washed in distilled water and incubated in 1% thiocarbohydrazide for 30 min at room temperature. Samples were then first x3 washed in distilled water and immersed in 2% osmium tetroxide for 30 min at room temperature; the samples were washed again x3 in distilled water. Samples were contrasted with 1% aqueous uranyl acetate for 30 min at 4 °C and washed 3x in distilled water. A solution of 0.06% lead nitrate was prepared by dissolving in aspartic acid (pH 5.5) at 60 °C which was then filtered and added to samples for 20 min at 60 °C before washing 3x with distilled water at room temperature. Cells underwent serial dehydration by immersing in each increasing ethanol concentration twice (30%, 50%, 70%, 90%, and 100%) and irradiating for 40 s at 250 W in a Pelco microwave. Samples were infiltrated with increasing concentrations of epon LX112 resin (25%, 50%, and 75%) in ethanol for 3 min at 250 W under vacuum in a Pelco microwave, then twice in 100% resin before

polymerising at 60 °C overnight. Ultrathin sections (~60 nm thick) were viewed in a JEOL1011 transmission electron microscope at 80 kV, and images captured at a primary magnification of 25kx (4 K × 4 K Soft Imaging camera; Morada; Olympus with iTEM software). Random images were captured systematically at a primary magnification of 25kx. Analysis was performed in a blinded manner on coded sets of images. A contact point between ER and mitochondria was defined by a distance of ≤25 nm between the membranes.

2.5. Proximity ligation assay (PLA)

To determine the number of ER-mitochondria contacts both with and without the presence of 2DG, the PLA assays (Sigma—Aldrich, Cat. No. DUO92008) using antibodies against IP3R1, PTPIP51 (mitochondria) and Grp75, VAPB (ER) mitochondria was performed according to the manufacturer's protocol. Images were captured using a fluorescent microscope (Zeiss Axioskop 2 Mot Plus, Carl Zeiss Microimaging Inc., Jena, Germany) and the number of PLA positive spots was quantified using the particle analysis function of ImageJ software (National Institutes of Health, MD, USA, https://imagej.nih.gov/ij/, 1997—2018) and expressed as the number of foci per cell.

2.6. Calcium imaging

Cells were loaded with 2 μM Fura-2 (Abcam, Cambridge, UK) for 1 h at 37 °C and 20 min at RT or 2 μM Rhod 2-AM (Abcam, Cambridge, UK) for 20 min at 37 °C, and fluorescence intensity was monitored on the Spark Multimode Microplate Reader (Tecan, Männedorf, Switzerland) at Ex/Em 340/510 nm and Ex/Em 380/510 nm for Fura-2, and Ex/Em 552/581 for Rhod-2AM.

2.7. Determination of mitochondrial ROS

Mitochondrial superoxide radicals in HBEC3 and B3 cells were detected using the MitoSOX Red Mitochondrial Superoxide Indicator (Thermo Fisher, Australia, Cat. No. M36008). Cells were treated with 5 μM MitoSOX and incubated at 37 °C for 10 min as per instructions provided with the kit. The cells were washed three times with a KSFM medium to remove any traces of MitoSOX before imaging. Live-cell imaging was performed using a confocal microscope (Zeiss LSM 700, Zeiss) at room temperature with the 561 nm laser line. Images were exported as '.TIFF' files and analysed using ImageJ software (National Institutes of Health, MD, USA). For quantification of the mitochondrial superoxide levels, regions enclosing the whole field of vision with cells were defined as regions of interest, and mean fluorescence intensity was determined. Finally, the figures were assembled into panels using Adobe Illustrator (Adobe Inc., CA, USA).

2.8. Measurement of oxygen consumption rates (OCRs)

Oxygen consumption rates of cells were determined using the Seahorse XF Analyzer (Agilent Technologies, CA, USA). Cells were incubated in a DMEM with 1 mM pyruvate, 2 mM glutamine, and 10 mM glucose in a CO_2-free incubator and treated with 2DG for 1 h +/− C7. After basal OCRs were assessed, OCR responses after the addition of oligomycin (1.5 μM), carbonyl cyanide 4-(trifluoromethoxy) phenylhydrazone (FCCP; 2 μM), and the mix of antimycin a (0.5 μM) and rotenone (0.5 μM) (XF Cell Mito Stress Kit, Seahorse Bioscience) were determined. OCRs were then normalized to the protein concentration and analysed using the Seahorse Wave Software 2.6.

2.9. Mitophagy detection

To detect mitophagy in cells cultured with or without 2DG, the Mitophagy Detection Kit, Mtphagy Dye (Dojindo Molecular Technologies, MD, USA) was used. Briefly, the cells were cultured on μ-slide 8 well (Ibidi GmbH, Planegg, Germany) and incubated with 100 nmol Mtphagy Dye diluted in KSFM for 30 min at 37 °C. Cells were subsequently washed with 1XPBS and treated accordingly with or without 2DG. As a positive control, the induction of mitophagy was performed by adding 100 μM carbonyl cyanide-4-(trifluoromethoxy) phenylhydrazone (FCCP). The cells were imaged using the confocal microscope at 561 nm (Ex) and LP 650 nm (Em). An increase in Mtphagy Dye-specific fluorescence intensity indicated mitophagy.

2.10. cDNA synthesis and quantitative RT-PCR

Total RNA was isolated from cells using TRIzol (Ref. 15,596,018; Thermo Fisher Scientific, Australia) according to the manufacturer's protocol. In the last step of RNA extraction, RNA was eluted in 50 μl of elution buffer and quantified using a Nanodrop ND-2000 Spectrophotometer (Thermo Fisher Scientific, Australia).

cDNA was synthesized using 1 μg RNA with a Sensiscript Reverse Transcriptase Kit (Cat. No. 205211; Qiagen, Australia) as per the manufacturer's instructions. Briefly, RNA, dNTPs, and random oligodT were added and incubated at 70 °C for 10 min before the addition of the Sensiscript reverse transcriptase enzyme. The reaction mixture was incubated at 37 °C for 1 h before thermocycling. Quantitative RT-PCR (qRT-PCR) was performed on 1—10 ng of cDNA using PowerUp SYBR Green Master Mix (Cat. No. A25742; Thermo Fisher Scientific, Australia).

The sequences of primers used in the current study are shown in Table 1.

qRT-PCR thermo-cycling was performed on QuantStudio 3 (Applied Biosystems, Thermo Fisher Scientific, Australia) as follows: Uracil-DNA glycosylase (UDG) activation at 50 °C for 2 min, Dual-Lock DNA polymerase activation at 95 °C for 2 min, denaturation at 95 °C for 15 s and annealing at 55 °C for 1 min; 40—50 cycles.

2.11. Measurement of mitochondrial fuel usage in cells (OCRs)

Percentage mitochondrial fuel usage of cells was determined using the Seahorse XF Analyzer (Agilent Technologies, CA, USA). Cells were incubated in a DMEM with 1 mM pyruvate, 2 mM glutamine, and 10 mM glucose in a CO_2-free incubator and treated with 2DG and 2DG + C7 for 1 h. After basal mitochondrial fuel usage was assessed, percentage mitochondrial fuel usage relative to glutamine, fatty acid, and glucose were assessed after the addition of 3 μM BPTES (an allosteric inhibitor of glutaminase). Glutaminase converts glutamine to glutamate, which is then converted to alpha-ketoglutarate before being oxidized in the TCA cycle), 4 μM of Etomoxir (an inhibitor of long-chain fatty acid oxidation) and 2 μM of UK5099 (an inhibitor of the glucose oxidation pathway). Percentage mitochondrial fuel usage relative to glutamine, fatty acid, and glucose were subsequently normalized to basal mitochondrial fuel usage and analysed using the Seahorse Wave Software version 2.6.

Table 1 — Primer sequences used for qRT-PCR.

Gene	Forward Primer (5′-3′)	Reverse Primer (5′-3′)
LDHA1	GTTGGTGCTGTTGGCATGG	TGCCCCAGCCGTGATAATGA
IDH1	AGGTTTTACTGGTGGTGTTCAGA	CCGCTCCTCCCACTGAATAG
KDGH1	CAGCTGATGAGGGCTCCG	CCTCTCTCTGGGCCTTACCT
MDH1	CTGCTTCCAAGTCAGCTCCA	CTCCCTCTGGGGTTCCAAAC
SDH1	ACTGTTGCAGCACAGCTAGA	GGCACTCCCCATTCTCCATC
PDH1	TTCTCAGAACCCGGCAAGC	AGCACTGTTGTGACAGGAGG
GAPDH	TCGGAGTCAACGGATTTGGT	TTCCCGTTCTCAGCCTTGAC

2.12. Measurement of ATP production rate

Data were derived from the efflux of hydrogen ions (Extracellular Acidification Rate, ECAR) and oxygen consumption (Oxygen Consumption Rate, OCR) of cells obtained during the Mito Stress Test following the equation below:

ATP production rate (pmol ATP/min) = Proton Exchange Rate, PER final (pmol H^+/min)

PER final (pmol H^+/min) = overall PER (pmol H^+/min) − mitoPER (pmol H^+/min)

Overall PER (pmol H^+/min) = ECAR (mpH/min) x BF (mmol H+/L/pH) x microchamber volume in XF 9 (μL) x Kvol

Mito PER (pmol H^+/min) = mitoOCR (pmol O_2/min) x CCF (pmol H^+/pmol O_2)

MitoOCR (pmol O_2/min) = OCR basal (pmol O_2/min) - OCR (upon addition of Rot/AA) (pmol O_2/min)

2.13. Extraction of intracellular metabolites for mass spectrometry

A protocol for the extraction of intracellular metabolites was adapted and modified from a previous study [31]. Briefly, after treatments, cells were washed twice with cold 1X PBS to quench metabolic reactions and to remove extracellular metabolites from the supernatant. Cells were collected in conical tubes by scraping and centrifuged at 0.3 RCF(Relative Centrifugal Force) to pellet the cells. The cell pellet was resuspended in 2 mL of cold 50% acetonitrile containing 250 nM azidothymidine as internal standard. The cells in the solution were lysed by freeze-thawing, vortexing, and sonication to release intracellular contents. The solution was then centrifuged at 4 °C at top speed to create a two-phase solvent—solvent extraction step. From the aqueous supernatant, 1.5 mL was recovered, avoiding the buffy coat layer containing cell debris and precipitated proteins. The aqueous fraction containing the metabolites was then freeze-dried. Fifty 50 μL sample was added into HPLC glass inserts for MS analysis.

2.14. MS of intracellular metabolites

Intracellular metabolites were analysed using liquid chromatography-tandem mass spectrometry (LC-MS/MS) [31—34]. Analyses were performed using a Dionex Ultimate 3000 HPLC system coupled to an AB Sciex 4000 QTRAP mass spectrometer. Liquid chromatography was performed using a 50 min gradient with 300 μL/min flowrate, on a Phenomenex Gemini-NX C18 column (150 × 2 mm, 3 μm, 110 A), with a guard column (SecurityGuard Gemini-NX C18, 4 × 2 mm), and column temperature of 55 °C. The mobile phases used were: 7.5 mM aqueous tributylamine (Merck) with the pH adjusted to 4.95 (±0.05) using acetic acid (Labscan) for Solvent A, and acetonitrile (Merck) for Solvent B. Samples were kept at 4 °C in the autosampler and 10 μL of various dilutions of samples were injected for analyses. The HPLC was controlled by Chromeleon 6.80 software (Dionex). Mass spectrometry was achieved using the scheduled multiple reaction monitoring (sMRM) method on the negative ionization mode. Other hardware parameter values were ion spray voltage −4500 V, ion source nebulizer (GS1), ion source auxiliary (GS2), curtain (CUR), and collision (CAD) gases were 60, 60, 20, and medium (arbitrary units), respectively, using an in-house ultra-high purity liquid nitrogen tank (BOC). The auxiliary gas temperature was kept at 350 °C. The mass spectrometer was controlled by Analyst 1.6.3 software (AB Sciex). Amounts obtained for each metabolite detected were based on standard curves from serial dilutions of analytical standards purchased from Merck Inc. Standard and pooled samples were regularly injected along the run sequence for quality control. Collected data were processed using MultiQuant 2.1 (AB Sciex).

2.15. Statistical analysis

Graph plotting and statistical evaluations of datasets were performed using GraphPad Prism version 8 (GraphPad Software, CA, USA). Both Student's t-test and nonparametric analyses were used to evaluate statistical comparisons in HBEC3-KT and B3 quantitation studies. Differences were considered to be significant if $p < 0.05$, 2-tailed t-tests. Data are presented as the mean ± s.d. from at least three separate experiments run in triplicate.

3. RESULTS

3.1. Correction of nutrient stress hypersensitivity in ATM-deficient and primary A-T cells by heptanoate

We showed previously that disruption of the ATM gene in the bronchial epithelial cell line (HBEC) to yield the cell line B3 led to metabolic stress and hypersensitivity to glycolysis inhibition in these ATM-deficient cells [26]. Our objective was to attempt to correct a series of metabolic defects in the ATM-deficient cells using the anaplerotic compound, heptanoate (C7). The reasoning was that replenishment of mitochondrial function by increasing TCA cycle activity would rescue ATM-deficient cells from this form of cell killing. The results shown in Figure 1A confirm that ATM-deficient (B3) cells are hypersensitive to glycolysis inhibition (2DG treatment) compared to control HBEC cells. C7 reduced the extent of cell killing to values comparable to those of controls (Figure 1A). We had also demonstrated previously that primary airway epithelial cells from patients were hypersensitive to nutrient deprivation as well as oxidative stress [12,26]. Therefore, we determined whether C7 correction might extend to patients' cells. Here we showed that airway epithelial cells from two different A-T patients showed approximately the same extent of cell death after 2DG treatment as the ATM-deficient cell line B3 (Figure 1B). Again, in the case of the A-T primary cells heptanoate reduced cell killing to levels comparable to control. We also showed that glucose-deprived olfactory neurosphere (ONS)-derived cells from A-T patients were protected by C7 (Figure 1C)

Previous results have demonstrated that ATM is a sensor of oxidative stress [35]; A-T cells are hypersensitive to ROS [12]. The absence of ATM is associated with elevated levels of ROS [26,36] and antioxidants protect A-T cells and increase the lifespan of $Atm^{-/-}$ deficient mice [17,37]. Accordingly, we determined whether ROS was generated under nutrient stress which could account for the increased cell killing in ATM-deficient cells, and investigated whether heptanoate could reduce ROS. Elevated basal ROS levels were evident in ATM-deficient cells compared to control and these were increased further after 2DG treatment (Figure 1D). Quantitation of ROS showed that levels were significantly higher in ATM-deficient cells under basal and 2DG-induced conditions (Figure 1E). Incubation of cells with heptanoate led to a significant reduction in ROS levels in both control and ATM-deficient cells (Figure 1C and D). We also showed that ROS was elevated in airway epithelial cells from A-T patients exposed to 2DG and that heptanoate significantly reduced this (Supp. Figure 1A and B). Since nutrient stress led to ROS generation which could account for some of the hypersensitivity in ATM-deficient cells, we next investigated whether antioxidants might also reduce cell killing brought on by nutrient stress. Figure 1F shows that N-acetyl cysteine (NAC) has a delayed and partially protective effect against glycolysis inhibition-induced cell killing in ATM-deficient cells. We showed that NAC was functioning under these conditions by its capacity to reduce MitoSOX labelling in these cells and thus protect them against cell killing. Failure of NAC to prevent ATM activation after 2DG treatment suggested that ROS may not be the activating factor but played a role in cell killing

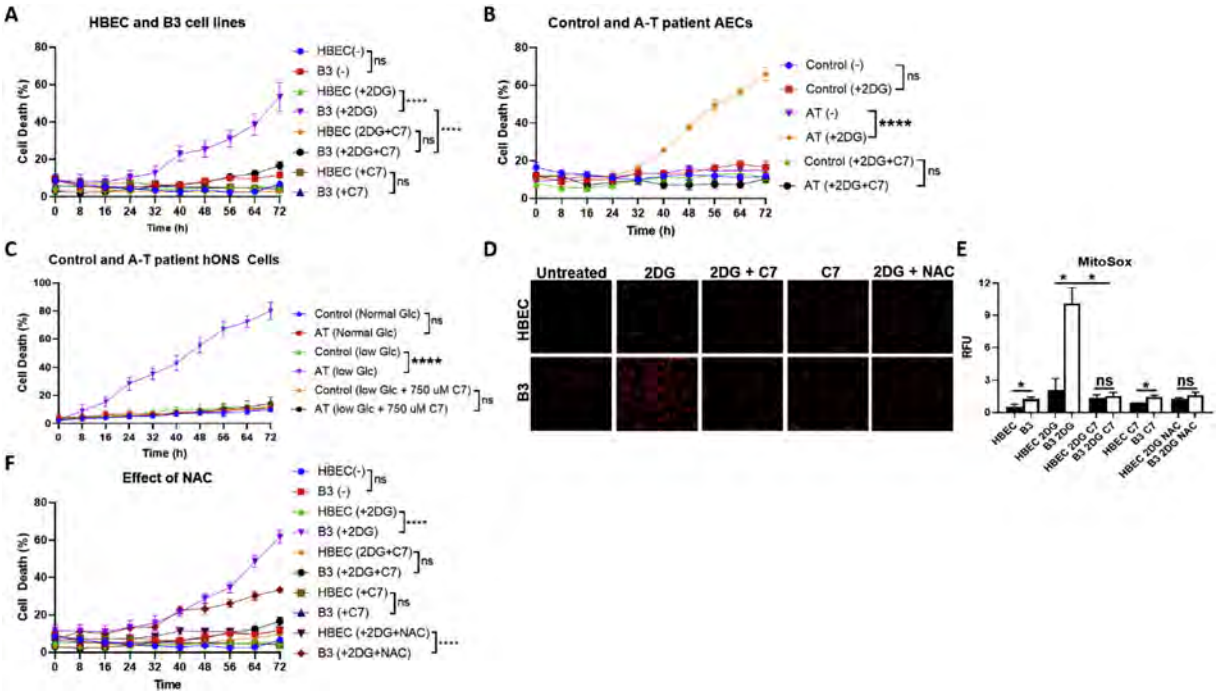

Figure 1: Correction of hypersensitivity to nutrient stress (glycolysis inhibition) and elevated ROS in A-T cells by heptanoate (C7). (A) Correction of sensitivity to nutrient stress in ATM-deficient cells by C7. HBEC (control), B3 (ATM-deficient cells generated by CRISPR/Cas9). 2DG, 2 deoxy glucose; C7, heptanoate. (B) Correction of sensitivity to nutrient stress by C7 in primary airway epithelial cells. Mean of two controls (C215, C218) and two A-T patient cells (AT009, AT014). (C) Correction of sensitivity in glucose-deprived olfactory neurosphere (ONS)-derived cells by C7. (D) Determination of mitochondrial ROS using MitoSOX labelling. NAC, N-acetylcysteine anti-oxidant. (E) Quantitation of the MitoSOX data was carried out by measuring fluorescence intensity for at least 4 separate determinations of cells in defined areas. (F) Correction of cell survival in control and ATM-deficient cells in response to NAC co-treatment with 2DG. C7 is included as a positive control. Scale bar, 5 μm. All data are plotted as mean +/− SEM. n ≥ 3, *p < 0.05 and ns for p > 0.05 using unpaired two-tailed Student's t-test (E) and two-way ANOVA (A,B,C and F).

[26]. However, replenishment of mitochondria with heptanoate metabolites is significantly more effective in protecting against this form of cell killing (Figure 1F).

3.2. Rescue of ER-mitochondrial interaction in ATM-deficient cells

ER-mitochondrial local interaction is essential for aspects of cell function and survival in mammalian cells [38,39]. We previously showed that the number of contact sites between ER and mitochondria is approximately the same in control and ATM-deficient cells but in response to nutrient stress, while they increase significantly in controls, that was not the case for ATM-deficient cells which may account for the greater sensitivity to nutrient stress [26]. Since heptanoate protected against cell killing in ATM-deficient cells, we determined whether it might also alter ER-mitochondrial contact points after exposure to stress using transmission electron microscopy (TEM) as a means of measuring the interaction between these organelles. As reported previously, the number of contact sites between mitochondria and ER were similar in untreated control and ATM-deficient cells but after 2DG they increased significantly only in control cells (Figure 2A and B). On the other hand, when the presence of heptanoate led to a significant increase in mitochondrial-ER contact points in ATM-deficient cells (Figure 2B). Since tight contacts between the ER and mitochondria facilitate delivery of Ca^{2+} to mitochondria we investigated VAPB and PTPIP51 tethering proteins that mediate the formation of these contacts 41, 42]. We initially employed the same immunofluorescence approach as reported previously for IP3R1-GRP75-VDAC1 bridge formation to study these tether proteins [26]. Again, in this case, 2DG treatment led to a marked increase in intensity for both VAPB and PTPIP51 in control cells over that observed in untreated cells (Figure 2C—E). However, the stress response was much less marked in ATM-deficient cells but treatment with heptanoate caused an increase in the intensity of both proteins in 2DG-treated cells which was comparable to that in control-treated cells (Figure 2C—E). To confirm whether this change resulted from tethering between VAPB and PTPIP51, we carried out PLA to investigate the proximity of these two proteins to each other. The results showed a significant increase in cytoplasmic puncta in control cells after 2DG treatment, illustrating an increased physical association between VAPB and PTPIP51, consistent with the increased ER-mitochondrial contact sites (Figure 2F and G). On the other hand, there was only a negligible increase in cytoplasmic puncta in ATM-deficient cells after 2DG treatment (Figure 2F and G). However, when treated with heptanoate, the cytoplasmic puncta increased significantly in 2DG-treated ATM-deficient cells to levels comparable to those in control cells (Figure 2F and G). Furthermore, as determined by immunoblotting, no increase was noted in levels of VAPB or PTPIP51 in control cells after 2DG treatment which might have accounted for an increased interaction (Figure 2H, Supp. Figure 2A and B)

Enhanced number of contact sites and increased tethering in ATM-deficient cells after treatment with heptanoate would be expected to lead to increased interaction between the organelles and Ca^{2+} transfer. Thus, we determined whether heptanoate treatment led to the efficient assembly of the IP3R1-GRP75-VDAC1 complex for Ca^{2+} transfer between the organelles. As shown in Figure 3A, 2DG treatment led to a marked increase in GRP75 intensity above basal levels which merged with the mitochondrial import receptor subunit (TOMM20) staining in control cells. This increase in intensity was not evident in ATM-deficient cells. On the other hand, ATM-deficient cells

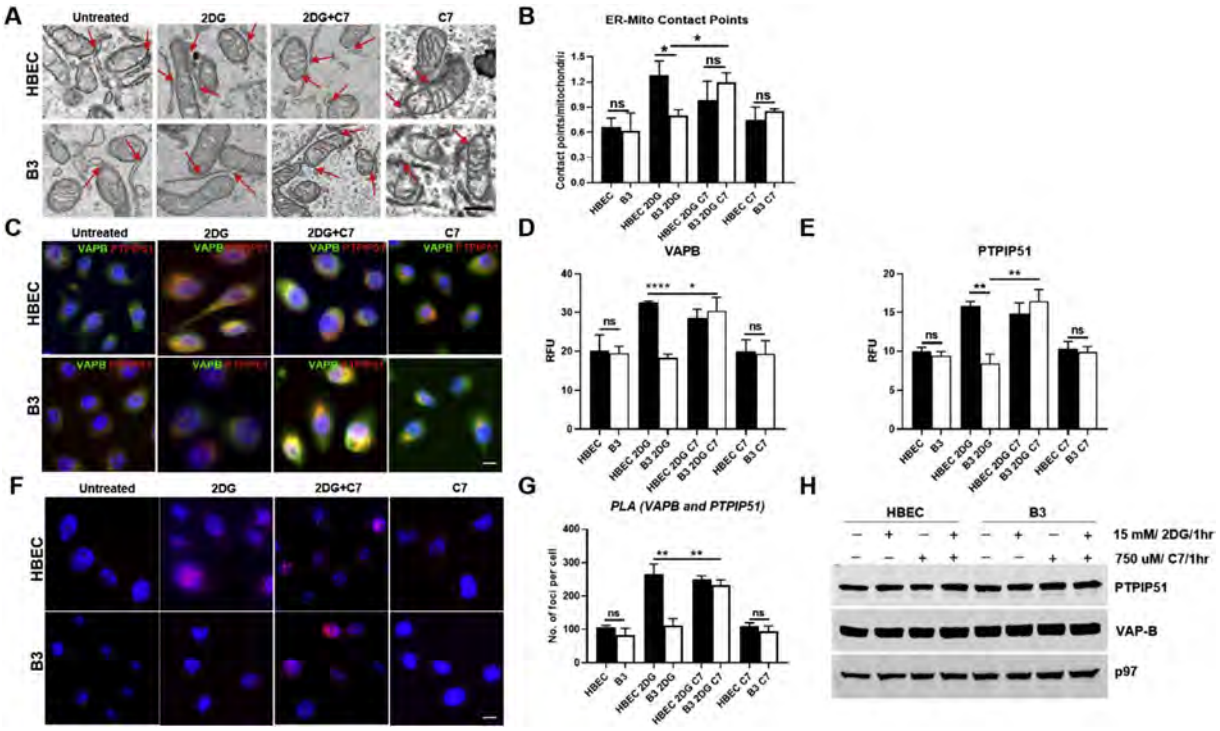

Figure 2: Correction of ER-mitochondrial contact sites in ATM-deficient cells by C7. (A) Electron microscopy of HBEC control and ATM-deficient B3 cells with and without exposure to 2DG +/− C7. A distance of 25 nm between mitochondria and ER is considered a contact. Each contact site is highlighted with a red arrow. An increase in the number of contact sites was observed in HBEC cells exposed to 2DG but not in B3, whereas the opposite was observed for B3. However, treatment with C7 significantly increased those in B3 to control levels, n = 3 experiments, 2DG and C7 treatments were done for 4 h. (C) Co-staining using an antibody against the ER protein VAPB (green) and the mitochondrial protein PTPIP51 (red) was performed on HBEC and B3 cells in the presence or absence of 2DG. An increase in the fluorescence intensity was observed in HBEC cells following exposure to 2DG and not in B3 but this was corrected by C7. (D) Quantitation of fluorescence intensity for VAPB (D) and PTPIP51 (E) were carried out on at least 10 separate determinations of cells in defined areas. (F) Proximity ligation assay (PLA) using antibodies against VAPB (ER) and PTPIP51 (mitochondria) was performed as a means of showing increased interaction between these two proteins in the presence of C7. An increase in the number of foci in HBEC cells following exposure to 2DG was observed but not in B3. In this case, also C7 enhanced the number of foci in 2DG -treated B3 cells. (G) Quantitation of the number of foci per cell. (H) Immunoblotting for PTPIP51 and VAPB in cells following exposure to 2DG and C7. p97 protein was used as a loading control. Scale bar, 5 μm. Negative control with no primary antibody was performed. All data are plotted as mean +/- SEM. $n \geq 3$, *$p < 0.05$, **$p < 0.01$, ****$p < 0.0001$ and ns for $p > 0.05$ using unpaired two-tailed Student's t-test.

treated with heptanoate showed a similar response to controls (Figure 3A). Quantitation of the data appears in Figure 3B. The increase in GRP75 fluorescence intensity is significant in 2DG-treated control cells, but very little change occurred for ATM-deficient cells. However, a very significant increase was observed in 2DG-treated, ATM-deficient cells where heptanoate was included during treatment (Figure 3B). As observed previously, ATM was activated by 2DG treatment (Figure 3E). These results suggest that heptanoate also rescues the defect in assembly of the IP3R1-GRP75-VDAC1 bridge in ATM-deficient cells. This is not explained by an increase in any of the three-member of the complex as revealed by immunoblotting (Figure 3E). To determine whether the increase in the intensity of GRP75 was due to increased linkage between the mitochondrion and the ER we also employed the proximity ligation assay (PLA) [42]. Here we examined the proximity between IP3R1 on the ER and GRP75 on the mitochondrion. We observed an increase in punctate cytoplasmic labelling in control cells after treatment with 2DG, revealing an increased interaction between IP3R1 and GRP75, confirming an increase in the number of IP3R1-GRP75-VDAC1 contacts between the ER and mitochondria (Figure 3C). As reported previously, only a small increase in cytoplasmic puncta was evident in ATM-deficient cells. However, when heptanoate was included during 2DG treatment the number of puncta in ATM-deficient cells increased dramatically to an intensity comparable to control (Figure 3C). Quantitation revealed that there was no significant increase in puncta over the baseline in ATM-deficient cells treated with 2DG, still the presence of heptanoate led to a significant increase (Figure 3D). These data demonstrate that heptanoate also enhances contact between GRP75 and IP3R1 in ATM-deficient cells, thus increasing ER-mitochondrial contacts. Furthermore, immunoblotting did not show a significant increase in either IP3R1, GRP75, or VDAC1 in control HBEC cells after 2DG treatment; it suggested that the increased protein levels do not contribute to the increased interaction among these proteins (Figure 3E). It is evident that under these conditions ATM is activated as described previously (26, Supp. Figure 3). Overall, these results reveal that the heptanoate increased the number of ER-mitochondrial contact points in ATM-deficient cells. Consistent with this, we observed increased ER-mitochondrial tethering between VAPB and PTPIP51 and an increase in the IP3R1-GRP75-VDAC1 Ca^{2+} channel.

3.3. Correction in Ca2+ signalling between ER and mitochondria in ATM-deficient cells in response to metabolic stress using heptanoate

Regulation of mitochondrial Ca^{2+} uptake is complex and depends on several different processes including release from the ER, contacts between the ER and mitochondria as well as control of the mitochondrial uptake machinery all of which are of key importance in cell death and survival [43,44]. We previously showed reduced interaction

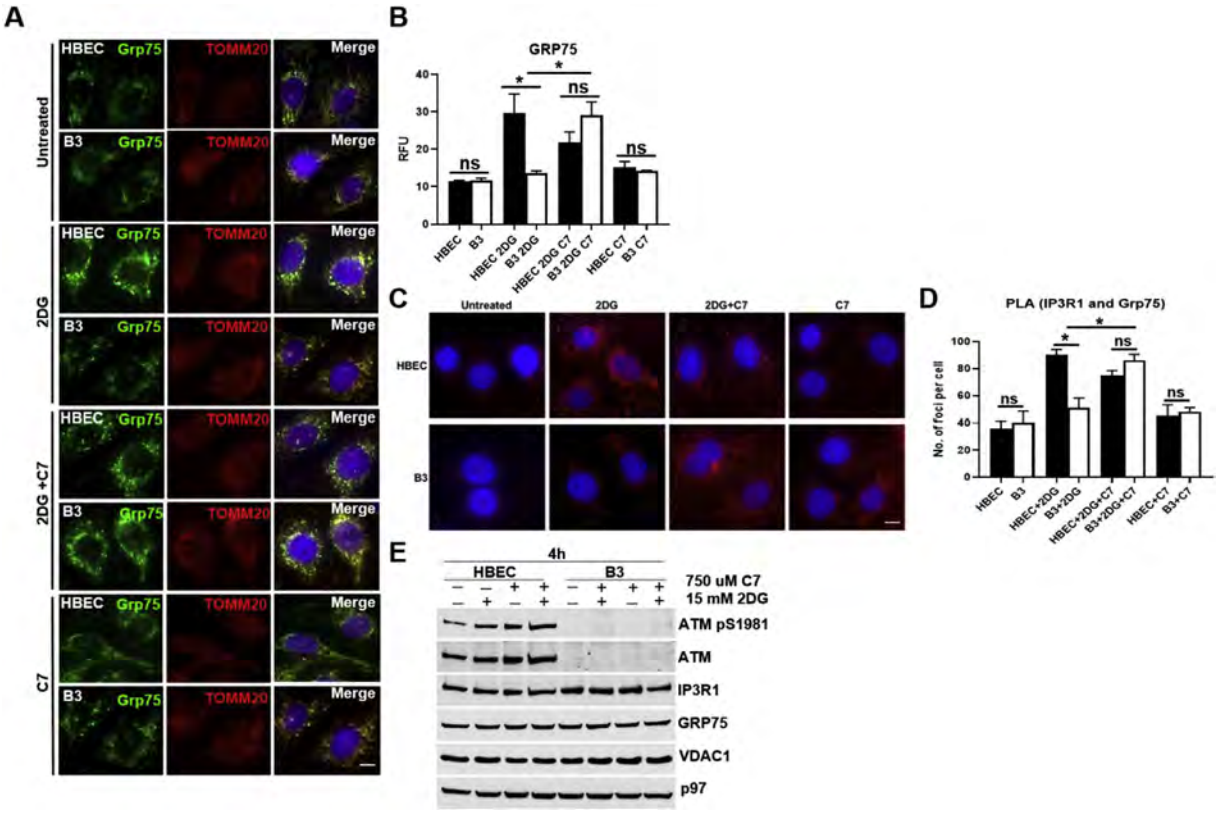

Figure 3: Effect of C7 on the IP3R1-GRP75-VDAC1 Ca^{2+} channel between ER and mitochondria. (A) Co-staining using an antibody against Grp75 (green) and TOMM20 (red) was performed on HBEC and B3 cells in the presence or absence of 2DG and C7. An increase in the fluoresce intensity was observed in HBEC cells following exposure to 2DG and not in B3 but the signal was enhanced to control levels in these cells in response to C7. (B) Quantitation of fluorescence intensity for Grp75 shows that C7 significantly increased the intensity of GRP75 labelling in ATM-deficient cells treated with 2DG, Scale bar, 5 μm (C) Proximity ligation assay (PLA) was also carried out here to confirm increased interaction between GRP75 and IP3R1. Unlike that in HBEC cells, an increase in the number of foci in ATM-deficient cells was not observed after 2DG but in the presence of C7, the number of foci was comparable to 2 DG-treated controls. (D) Quantitation of PLA foci per cell. Scale bar, 5 μm. (E) Immunoblotting for Grp75, IP3R1, and VDAC1 in cells following exposure to 2DG and C7 treatment again confirmed ATM activation after nutrient stress but showed no differences in IP3R1-GRP75-VDAC1 protein levels after 2DG treatment or when C7 was added. p97 protein was used as a loading control. All data are plotted as mean +/− SEM. $n \geq 3$, *$p < 0.05$, ns for $p > 0.5$ using unpaired two-tailed Student's t-test.

between ER and mitochondria in ATM-deficient cells in response to metabolic stress and demonstrated that there was a defect in Ca^{2+} release from the ER and transfer to mitochondria under these conditions [26]. The basal level of release of Ca^{2+} from the ER was approximately the same in both cell types but on exposure to 2DG, a rapid release occurred into the cytoplasm for HBEC control cells, but it was significantly reduced in ATM-deficient cells (Figure 4A). However, when heptanoate was included in metabolically stressed ATM-deficient cells it significantly increased the release of Ca^{2+} to levels comparable to those of controls (Figure 4A). A small but non-significant increase was observed in control cells incubated with heptanoate and 2DG, presumably because maximal levels were achieved under nutrient stress alone. We also showed previously that the release of Ca^{2+} from the ER and its subsequent uptake into mitochondria to achieve Ca^{2+} homeostasis was also defective in ATM-deficient cells. Here again, we demonstrated the same phenomenon, that ATM-deficient cells are also

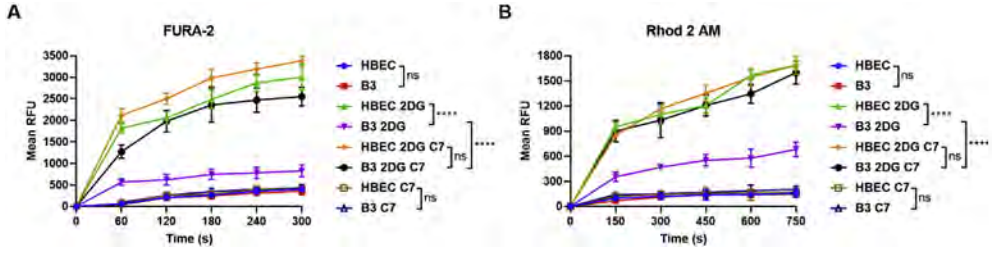

Figure 4: Correction of Ca^{2+} transfer between ER and mitochondria in ATM-deficient cells by C7. (A) Determination of intracellular calcium using FURA-2, a sensitive indicator for Ca^{2+} largely released from intracellular ER stores. While the release was deficient in ATM-deficient cells after 2DG treatment this was restored to control levels in the presence of C7. (B) In order to determine Ca^{2+} uptake into mitochondria, we employed Rhodamine-2AM a cationic fluorescent dye that labels respiring mitochondria. Similar results to those with FURA-2 were observed., a significant increase in calcium uptake occurred in ATM-deficient treated with 2DG in the presence of C7 indicating that C7 corrected both release and uptake of Ca^{2+}. All data are plotted as mean +/− SEM. $n \geq 3$, ****$p < 0.0001$, ns for $p > 0.5$ using two-way ANOVA.

defective in the uptake of Ca^{2+} into mitochondria compared to control (Figure 4B). Furthermore, the inclusion of heptanoate after 2DG treatment in ATM-deficient cells produced levels of Ca2+ uptake comparable to control and the increase was of the same order as observed for Ca^{2+} release from the ER (Figure 4B). These results demonstrate that the defective linkage between the ER and mitochondria in ATM-deficient cells, in response to nutrient stress, and the significantly reduced release of Ca^{2+} from the ER and reduced uptake into mitochondria can be corrected by heptanoate.

3.4. Heptanoate corrects several aspects of mitochondrial dysfunction in ATM-deficient cells in response to nutrient stress

Evidence has been provided for intrinsic mitochondrial dysfunction in A-T cells [22,24], for a new role for ATM in regulating mitochondrial function and mitophagy [24,45], and for a role for ATM in mitochondrial redox sensing [35]. Senescence control by the lysosomal–mitochondrial axis is modulated by ATM activity [46] and ATM is activated by ATP depletion and regulates mitochondrial function through Nuclear respiratory factor 1 (NRF1) [25]. These results together with our previous findings that glycolysis inhibition exacerbates mitochondrial dysfunction in ATM-deficient cells highlight the importance of mitochondrial function to the A-T cellular phenotype. Though there is some controversy on the exact nature of the mitochondrial defect, we and others have provided evidence for a defect in oxygen consumption rates in different ATM-deficient cells [9,26]. We determined here whether heptanoate would correct the mitochondrial dysfunction in ATM-deficient cells. As observed previously maximal respiratory capacity was elevated in untreated B3 compared to control and incubation with 2DG led to a marked increase in maximal respiratory capacity per viable ATM-deficient cell compared to controls (Figure 5A). The inclusion of heptanoate led to a dramatic reduction in ATM-deficient cells to values the same as in treated controls (Figure 5B). The addition of heptanoate to untreated cells did not alter OCR (Figure 5C). When glycolysis is inhibited by 2DG in the presence of O_2 cells can still produce ATP through their mitochondria using alternate energy sources [47,48]. To determine whether there might be a change in fuel dependence in ATM-deficient cells, we performed Mito Fuel Flex Test using Seahorse XFe96. The results in Supp. Figure 4A show a greater dependence for glucose and fatty acids under basal conditions in ATM-deficient cells and this dependence is reduced after 2DG treatment. When C7 was included ATM-deficient cells showed an increased dependence on fatty acids as a fuel source compared to control as expected (Supp. Figure 4B). The C7 treatment on its own showed dependency levels comparable to those under basal conditions as expected (Supp. Figure 4C). Given the abnormalities in mitochondrial respiration in ATM-deficient cells we determined the effects of nutrient deprivation on ATP levels using a colorimetric assay. Surprisingly, we observed that ATP levels were significantly higher in untreated ATM-deficient cells than in controls (Figure 5D and E). On exposure to 2DG, these ATP levels showed a significant decrease in ATM-deficient cells than in controls at both 1 h and 5 h post-treatment (Figure 5D and E). This is consistent with ATP production rates (Supp. Figure 4D). Since 2DG inhibits glycolysis, these data suggest that glycolysis is being employed to a greater extent in ATM-deficient cells, consistent with our fuel dependence data (Supp. Figure 4). The inclusion of heptanoate rescued ATP levels in ATM-deficient cells consistent with improving mitochondrial respiration (Figure 5D and E). These results are consistent with recent observations that show that ATM deficiency leads to altered cellular metabolism and an enhanced level of aerobic glycolysis [25,49].

Blocking the separation of damaged mitochondria from healthy ones negatively affects mitophagy [50]. Previous data have also shown that the process of removing damaged mitochondria is defective in ATM-null fibroblasts, neurons, and ATM-deficient worm cells, and increasing intracellular NAD^+ is associated with improving mitochondrial quality via mitophagy [9,24]. We showed a significant increase in mitophagy in control cells treated with 2DG but that increase did not occur in ATM-deficient cells (Figure 5F). On the other hand, when heptanoate was included, it corrected the mitophagy defect in ATM-deficient cells (Figure 5F). These results show that the presence

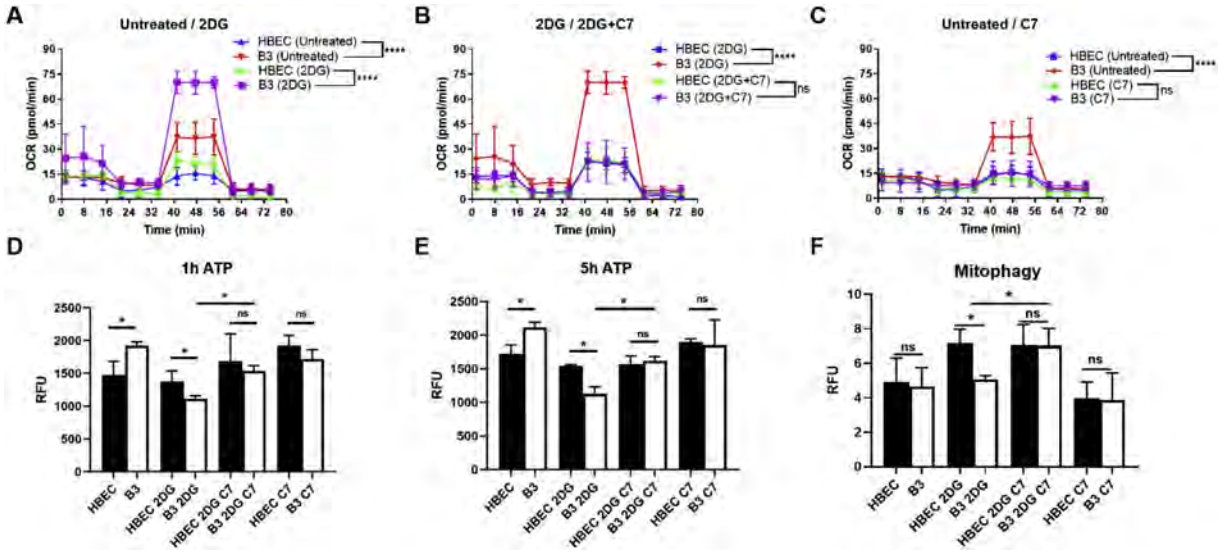

Figure 5: Correction of mitochondrial dysfunction in ATM-deficient cells by C7. (A) Mitochondrial function analysis was performed using the Seahorse XF24 extracellular flux analyser. 2DG causes a major increase in oxygen consumption rate (OCR) and respiratory capacity in ATM-deficient cells which was reduced to normal levels with C7 co-treatment. (C) Significant reduction in basal OCR by C7 in untreated ATM-deficient cells. (D) Determination of ATP levels at 1 h after exposure to 2DG in the presence and absence of C7. (E) Determination of ATP levels at 5 h after exposure to 2DG in the presence and absence of C7. ATP was assayed using a colorimetric method as described in Methods. All data are plotted as mean +/− SD, n ≥ 3, *p < 0.01, ns for p > 0.05 using two-way ANOVA (A, B and C) and unpaired two-tailed Student's t-test (D, E, and F).

of heptanoate corrects several parameters of mitochondrial dysfunction in ATM-deficient cells as well as increases mitophagy.

3.5. Effects of heptanoate on metabolic profile

The correction of ER-mitochondrial signalling and mitochondrial function in ATM-deficient cells by heptanoate is in keeping with its anaplerotic effect in replenishing TCA cycle intermediates and protecting against cell killing [27]. To investigate this in greater depth, we carried out a metabolic profile of relevant intermediates. A critical step in the pathway is the involvement of lactate dehydrogenase (LDH), an enzyme that catalyses the reversible conversion of lactate to pyruvate [51,52]. Specifically, the LDHA1 isoenzyme shows a greater affinity for pyruvate and mediates the preferential conversion of pyruvate to lactate [53,54]. We initially determined the expression of lactate dehydrogenase (LDHA1) as an indicator of greater reliance on aerobic glycolysis in these cells. The results in Figure 6A show that the basal level of expression of LDHA1 is significantly higher in ATM-deficient cells than in controls and exposure of these cells to 2DG led to a further and significantly greater increase in LDHA1 compared to controls (Figure 6A). On the other hand, when 2DG-treated cells were also exposed to heptanoate, a dramatic decrease in LDHA1 was observed in ATM-deficient cells to levels comparable to normal control cells (Figure 6A). The increased levels of LDHA1 in ATM-deficient cells should lead to significantly elevated lactate levels in these cells which turned out to be the case in both untreated as well as glycolysis inhibited ATM-deficient cells compared to controls (Figure 6B) These elevated levels of lactate in ATM-deficient cells were restored to normal levels with heptanoate (Figure 6B). Since LDHA1 mediates the preferential conversion of pyruvate to lactate, consistent with increased lactate levels, a significant decrease was seen in pyruvate levels in basal untreated and 2DG-treated ATM-deficient cells compared to controls (Figure 6C). Exposure of these cells to heptanoate restored the pyruvate levels to an extent that was approximately the same as in controls. These results correlate with reduced levels of pyruvate dehydrogenase 1 (*PDHA)* gene levels in ATM-deficient cells compared to controls (Supp. Figure 5A). The significant difference between controls and ATM-deficient cells became far more pronounced with 2DG treatment. However, co-treatment with C7 significantly improved the *PDHA* levels which are comparable to controls (Supp. Figure 5A). No significant differences were observed for several other TCA cycle-enzymes (Supp. Figure 5B—E). We suggest that the reduced pyruvate levels might reflect on levels of acetyl CoA. The results in Figure 6D showed that while acetyl CoA levels were comparable in untreated control and ATM-deficient cells,

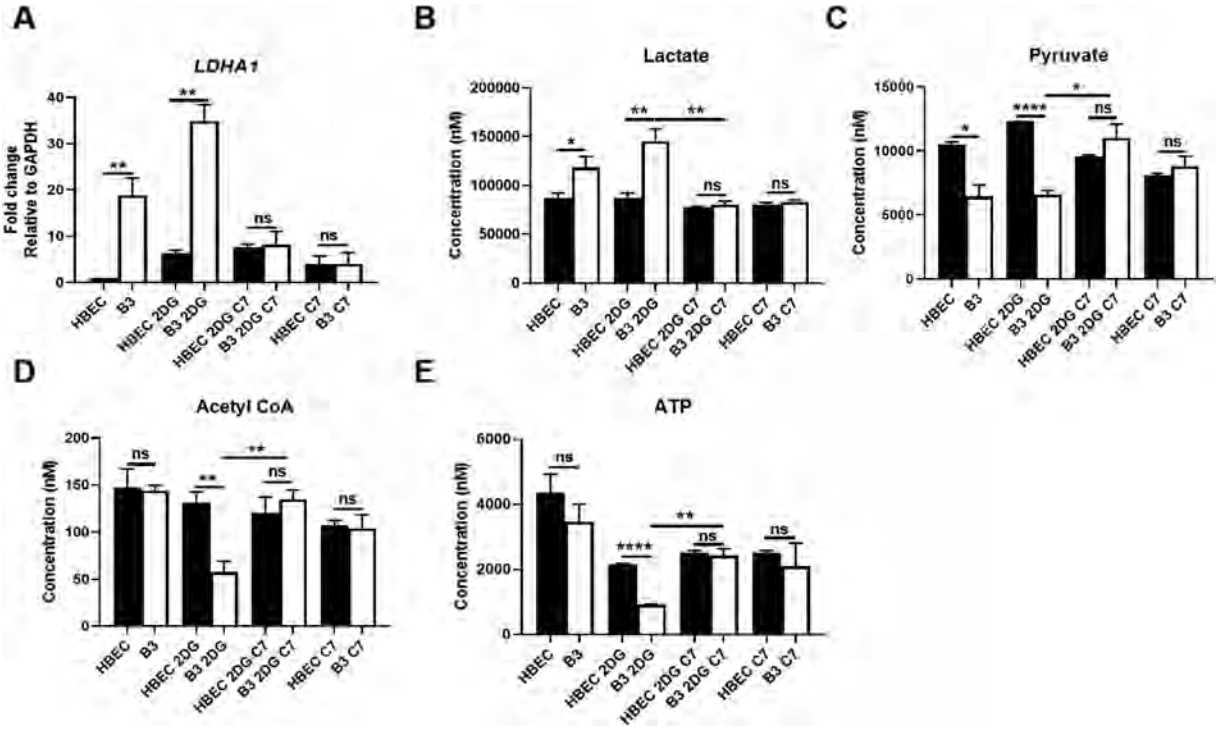

Figure 6: Metabolic analysis of glycolysis intermediates in 2DG and 2 DG + C7 treated cells. (A) Quantification of LDHA1 mRNA fold changes in HBEC and B3 cells was carried out by qPCR. Fold changes are shown as 2-ɗɗCt normalised to housekeeping gene GAPDH. *LDHA1* mRNA levels were ~20 fold higher in B3 cells which further elevated to ~35-fold with 2 DG treatment. Exposure to C7 treatment brought the *LDHA1* expression down to levels comparable to HBEC (~10-fold). (B) Quantitation of lactate levels in HBEC and B3 cells was carried out by LC-MS analysis. A significant increase in lactate levels was observed in untreated B3 cells compared to HBEC cells. Lactate levels were further enhanced in B3 cells treated with 2DG while the levels remained unaltered in HBEC cells. Exposure to C7 treatment brought down the lactate concentration in B3 cells to levels comparable to HBEC cells which were also similar to levels observed in untreated HBEC cells. (C) Quantitation of pyruvate levels in HBEC and B3 cells. Pyruvate levels were significantly lower in untreated B3 cells compared to HBEC controls. Pyruvate levels increased significantly in response to 2DG treatment in HBEC cells whereas the levels remained unaltered in B3 cells. Exposure to C7 treatment caused a significant increase of pyruvate concentration in B3 cells to levels comparable to HBEC controls. (D) Quantitation of acetyl CoA levels showed a significant decrease in B3 cells compared to HBEC cells. Exposure to C7 treatment caused a significant increase in acetyl CoA concentration in B3 cells to levels comparable to HBEC controls. (E) Quantitation of ATP showed a significant decrease in B3 cells compared to HBEC cells. Exposure to C7 treatment caused a significant increase in ATP concentration in B3 cells to levels comparable to HBEC controls. All data are plotted as mean +/− SEM. n ≥ 3, *p < 0.05, **p < 0.01, ***p < 0.001, ****p < 0.0001 unpaired two-tailed Student's t-test.

exposure to 2DG led to significantly reduced levels of this metabolite in ATM-deficient cells (Figure 6D). Furthermore, heptanoate restored levels of acetyl CoA in ATM-deficient cells to control levels consistent with its capacity to generate acetyl CoA. Other members of the TCA cycle as well as crucial enzymes involved in catalysing their conversions were also investigated by metabolomics and qRT-PCR, respectively. Significant differences were observed only for citrate levels after 2DG treatment which was corrected by C7 in ATM-deficient cells (Supp. Figure 6A–D). Based on these results we expected that the treatments would impact ATP levels. Using the more sensitive metabolic approach of LC/MS, ATP levels were found to be comparable in ATM-deficient and control cells (Figure 6E). However, when exposed to 2DG, the ATP levels in both control and ATM-deficient cells decreased as expected but to a significantly lower level in ATM-deficient cells consistent with the abovementioned results (Figure 6E). Again, as expected treatment with heptanoate partially corrected this effect by restoration to control cell levels (Figure 6E) Thus, all these changes including an increase in *LDHA1* and the correction in levels of metabolites in heptanoate-treated ATM-deficient cells suggested a shift to more reliance on mitochondrial oxidative metabolism which agrees with earlier results showing improvement in mitochondrial function in these cells (Figure 5).

4. DISCUSSION

A-T is a multisystem disorder where the majority of patients succumb to pulmonary dysfunction, cancer, and progressive neurodegeneration [55–57]. At present, there is no cure for A-T with patients being managed in a palliative manner by treatment of symptoms using immunoglobulin supplementation [56]. We describe here a potential approach to therapy through correction of mitochondrial dysfunction in A-T cells. The role of ATM in the DNA damage response has been widely reported and while other phosphatidyl-inositol 3 kinase-like kinases can partially substitute for ATM, their activation does not correct ATM deficiency [58]. Furthermore, ATM is involved in the repair of a subgroup of DNA DSBs and its specific role appears to be in preventing the re-joining of breaks by toxic non-homologous end-joining (NHEJ) and participating in DNA repair by homologous recombination (HR) [59]. While this provides insight into how ATM functions, it does not provide a ready approach to therapy. There is increasing evidence that A-T can be considered at least in part as a metabolic disorder which can account for some major characteristics of the disease as well as a variety of the lesser-known features including insulin resistance, diabetes, heart disease and heart failure, metabolic syndrome; oxidative stress and autophagy defect [60–64]. A common thread to these features is oxidative stress in which ATM is activated and recently described as a "neglected antioxidant" employing mitophagy to protect the cell against ROS [65]. Oxidative stress appears to be a universal characteristic of A-T and arises due to mitochondrial dysfunction. It has been suggested that the phenotype in A-T can, in part, be explained by a defect at the level of the mitochondrion [9]. Several reports support this including those on defective mitochondrial respiration in A-T lymphoblastoid cells [22], mitochondrial instability in fibroblasts [21], defective mitochondrial redox signalling [23], inactivation of Beclin-1 (regulator of autophagy) reverses mitochondrial abnormalities and tumour development in $Atm^{-/-}$ mice [9], and reducing mitochondrial ROS improves disease-related pathology in Atm-deficient mice [15,66]. In addition, loss of ATM induces mitochondrial dysfunction and compromises mitophagy due to NAD + insufficiency [24], ATM mediates spermidine-induced mitophagy via PINK1 and PARKIN regulation in human fibroblasts [45]; cells lacking ATM replenish ATP poorly following surges in energy demand which impacts on cell survival [25]. Based on these data, we reasoned that improving mitochondrial function might relieve the effects of metabolic stress on A-T cells and provide the basis for a novel approach to treatment at least of those aspects of the phenotype induced by mitochondrial dysfunction.

Our recent demonstration that ATM-deficient cell lines and airway epithelial cells from patients with A-T are hypersensitive to nutrient stress provided a useful model to investigate this [26]. We observed a 3-fold increase in sensitivity to glycolysis inhibition in ATM-deficient cells which is comparable to that in A-T cells exposed to ionizing radiation or oxidative stress [12,67–69]. While we have observed the hypersensitivity to nutrient stress in a variety of A-T cells we recognise that at this stage it is not possible to extrapolate this to all cell types affected in patients, e.g. Purkinje neurons in the cerebellum [1,2]. Our previous data suggested an association of this hypersensitivity to a defect in ER-mitochondrial signalling in A-T cells [26]. Since a multitude of published data and our recent results point to a defect in mitochondrial function in A-T cells, we concluded that compounds that enhanced mitochondrial function would be beneficial to patients' cells. We selected heptanoate, a metabolite of triheptanoin, an edible odd-chain fatty acid triglyceride, which is metabolized, in turn, to acetyl-CoA and propionyl-CoA, both of which enter the TCA cycle to replenish intermediates and supply energy to the cell [28]. Our results showed a complete correction of the cell-killing effect of glycolysis inhibition by heptanoate. Evidently, correcting mitochondrial dysfunction prevents cell killing arising from nutrient deprivation. This protective effect is observed both in ATM-deficient cells and in primary cells from patients. The actual mechanism of protection remains unclear since heptanoate reduces cell killing and also reduces mitochondrial-induced ROS. However, the removal of ROS per se does not appear to be responsible for this protection since the antioxidant NAC failed to prevent nutrient-deprivation–induced ATM activation at short times after treatment [26], suggesting that activation is not induced by ROS and instead by an unknown product/metabolite of nutrient stress. In addition, the inclusion of NAC in 2DG-treated ATM-deficient cells only partially protected these cells against death while heptanoate was more effective through its anaplerotic effects. The effect in reducing cell death is likely due to another consequence of improving mitochondrial function.

In addition to protecting against cell killing, heptanoate also corrected several steps in ER-mitochondrial signalling in ATM-deficient cells. The ER houses the major Ca^{2+} store in mammalian cells and this store is released through IP3R channels on the ER membrane [43]. Signalling crosstalk from the ER to the mitochondria is expected to be more efficient at tight interfaces and control of Ca^{2+} concentration within tight limits is of primary relevance to cell physiology [44]. Our previous data showed that there was a defect in the voltage-dependent anion channel IP3R1-GRP75-VDAC1 complex formation in ATM-deficient cells exposed to nutrient deprivation. This structure embedded in the mitochondrial-associated endoplasmic reticulum (MAM) is responsible for ER-mitochondrial tethering and transfer of Ca2+ ions from the ER to mitochondria [70]. It plays a key role in bridging between these organelles, functioning as an important determinant of cell fate under conditions of different forms of stress [71,72]. We showed here that the formation of this complex in A-T cells after nutrient stress was increased to control cell levels after

heptanoate treatment, as determined by quantitation by immunofluorescence microscopy, proximity ligation, and transmission electron microscopy. As part of the process of strengthening ER-mitochondrial contacts and maintaining this Ca2+ channel, we also observed 2DG-induced tethering between VAPB and PTPIP51, tethering proteins that mediate the formation of these contacts in control cells [40,41]. Though tethering was not increased in ATM-deficient cells in response to nutrient stress, it responded positively after heptanoate treatment. Heptanoate increased the number of ER-mitochondrial contact points at least in part by increasing VAPB-PTPIP51 tethering which in turn increased the controlled flow of Ca^{2+} ions between the two organelles taking it to levels comparable to that in control cells. The magnitude of the release of Ca^{2+} from the ER and its uptake into mitochondria in ATM-deficient cells, exposed to glycolysis inhibition and heptanoate, represented a 6-7-fold increase observed over that in the absence of heptanoate. The data show that heptanoate also increases the uptake into the mitochondrion which is consistent with the increased assembly of the IP3R1-GRP75-VDAC1 complex. The controlled release and uptake of Ca^{2+} are critical to cell survival since enhanced Ca^{2+} release from the ER can cause mitochondrial overload and cell death [73,74]. This is a novel finding for heptanoate since it shows that its anaplerotic activity can be explained not only by providing TCA intermediates to mitochondria but that it also functions by enhancing ER-mitochondrial contact, signalling Ca^{2+} transfer. Cardenas [75] showed that mitochondrial uptake of IP3R1-released Ca^{2+} is an essential cellular process required for efficient mitochondrial respiration and maintenance of normal cell bioenergetics.

We have previously shown that exposure of ATM-deficient cells to 2DG led to marked increases in oxygen consumption rates (OCRs) per viable cell compared to controls including an increase in basal respiration and a very significant increase in maximal respiratory capacity in these cells, possibly due to an increase in energy demand in an attempt to overcome glycolysis inhibition [26]. This is in agreement with data from *Atm*$^{-/-}$ thymocytes and fibroblasts both of which exhibit increased cellular respiration under basal conditions. The OCR was elevated in *Atm*$^{-/-}$ cells and *Beclin-1* heterozygosity significantly rescued this abnormality [9]. We showed that treatment with heptanoate rescued the elevated maximal respiratory capacity seen after glycolysis inhibition in ATM-deficient cells, thus providing evidence that this compound is correcting mitochondrial dysfunction to maintain normal bioenergetics [75]. This was further confirmed by comparing metabolic profiles in control and ATM-deficient cells. Increased levels of *LDHA1* in ATM-deficient cells indicated a greater reliance on aerobic glycolysis in these cells, which was exacerbated after 2DG treatment. Consistent with this, we observed increased lactate levels under both conditions in ATM-deficient cells compared to controls. Furthermore, heptanoate had a marked effect in reducing both *LDHA1* and lactate in ATM-deficient cells supporting an improvement in mitochondrial function. Significantly reduced pyruvate and acetyl CoA levels in 2DG -treated ATM-deficient cells were restored by heptanoate suggesting a shift to mitochondrial oxidative metabolism. Finally, restoration of ATP levels by heptanoate after inhibition of glycolysis was additional evidence in support of improvement in mitochondrial function. Previous results showed that ATM-deficient cells were less flexible in adapting to changes in energy demand [25]. While the rate of reduction of ATP in response to stress was the same in wild-type and ATM-deficient cells in that study, the rate of recovery was significantly slower. We observed a similar result here where ATP was still significantly lower 5 h after treatment of ATM-deficient cells (Figure 4F). Our results suggest that glycolysis is being used to a greater extent in ATM-deficient cells to meet energy demand. This is supported by recent results showing that ATM-deficiency altered cellular metabolism and enhanced the Warburg effect in prostate cancer cells [49]. This revealed that ATM deficiency shunted the glucose flux to aerobic glycolysis by upregulating *LDHA1* expression and generation of increased lactate. We made the same observation in ATM-deficient cells with evidence of a greater emphasis on aerobic glycolysis in these cells due to reduced mitochondrial function. Upregulation of *LDHA1* and increased production of lactate in the cytoplasm was also reported in response to ATP depletion in Atm-deficient cells [25]. In that study, loss of ATM showed to impair the TCA cycle and favor the conversion of pyruvate to lactate over acetyl-CoA. The results obtained here for ATM-deficient cells are consistent with the above observations favouring a greater reliance on aerobic glycolysis. Heptanoate restored levels of lactate, pyruvate, and acetyl-CoA to control levels in ATM-deficient cells exposed to nutrient stress and protected them from cell killing after inhibition of glycolysis. The failure to observe the normal conversion of pyruvate to acetyl CoA is supported by reduced levels of *PDHA1* in ATM-deficient cells. Previous data have also shown that the process of clearing damaged mitochondria is defective in ATM-deficient cells and that increasing intracellular NAD+ is associated with improving mitochondrial quality via mitophagy [9,24]. These results demonstrate that glycolysis inhibition exacerbates mitochondrial dysfunction in ATM-deficient cells. The capacity of this form of stress to cause accumulation of ATM on mitochondria further supports an extranuclear role for this protein [18,26].

These results suggest that the anaplerotic effects of heptanoate are more complex than only supplying intermediate to the mitochondrion. Once a mitochondrial function is restored by supplying these intermediates, it is further enhanced by improving signalling with other organelles. We show here that ER-mitochondrial crosstalk is increased in response to metabolic stress in the presence of heptanoate to supply Ca^{2+} and improves mitochondrial function (Figure 7). Thus, it protects ATM-deficient cells against hypersensitivity to nutrient stress-induced cell killing. The parent compound triheptanoin has been employed for the treatment of a range of metabolic disorders and other diseases where energy deficiency is implicated [27–30]. It received its first regulatory approval in June 2020 as a source of calories and fatty acids for the treatment of paediatric and adult patients with confirmed long-chain fatty acid oxidation disorders [28]. We consider an excellent candidate for the treatment of patients with A-T since it would be predicted to address the mitochondrial deficit in these patients. The importance of the mitochondrial abnormalities to the A-T cellular defect is evident from the hypersensitivity of these cells to glycolysis inhibition which is comparable to the degree of sensitivity of these cells to ionizing radiation which appears to be due to a reduced capacity to deal with DNA DSBs. The conventional view that the DNA DSB defect is responsible for the majority of the A-T phenotype is questionable given the response of ATM-deficient cells to metabolic stress that does not include damage to DNA. We hypothesize that the ER-mitochondrial defect we have seen in ATM-deficient cells could well be relevant to the propensity of Purkinje cells to die in A-T patients [2] since damage to ER-mitochondrial signalling contributes to synaptic dysfunction in neurodegenerative disease [41]. In addition, a recent report using single nucleus RNA sequencing of the human cerebellum identified upregulation of apoptotic and ER stress pathways in Purkinje neurons and revealed strong downregulation of Ca2+

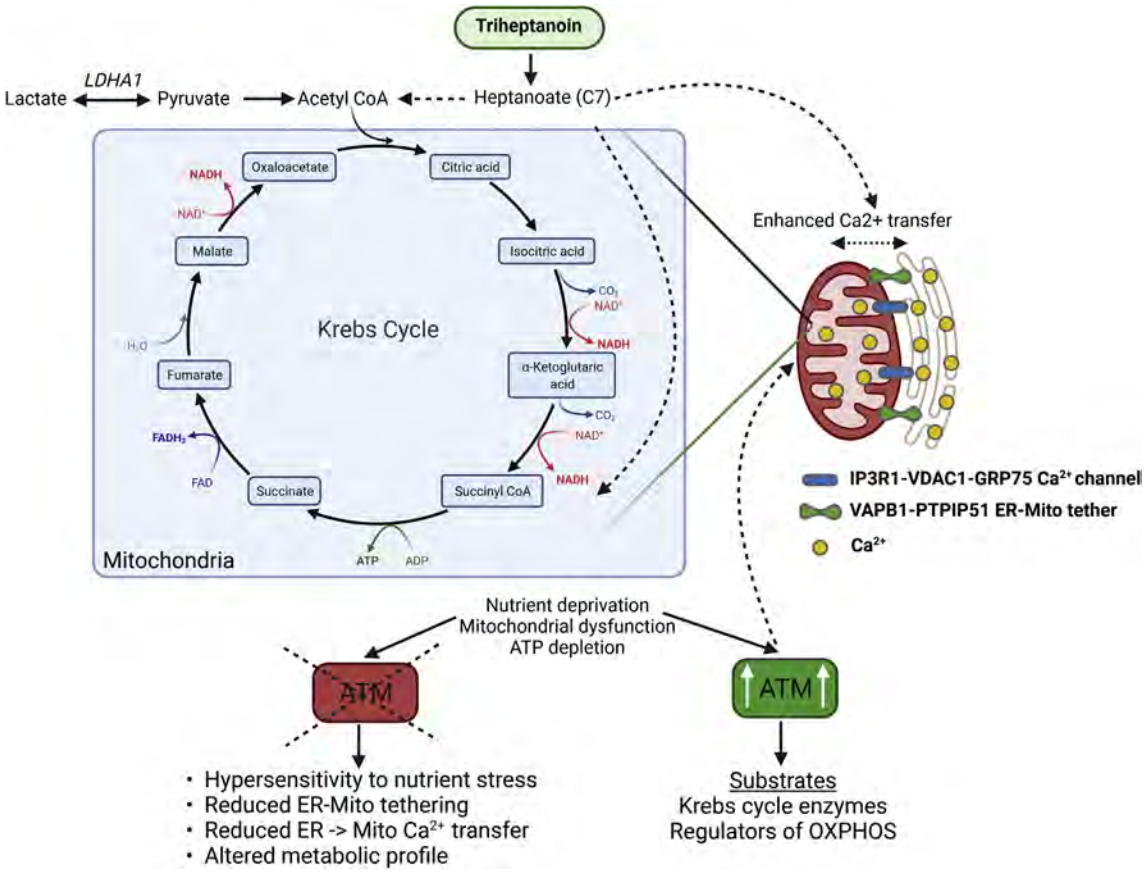

Figure 7: Anaplerotic effect of heptanoate in correcting the mitochondrial defect in ataxia-telangiectasia (A—T) cells. Inhibition of glycolysis with 2DG treatment and the resulting nutrient stress activates ATM and enhances ER-mitochondrial signalling for the transfer of Ca^{2+} between the two organelles. This signalling is deficient in A-T cells rendering them hypersensitive to this form of metabolic stress. Co-treatment of ATM-deficient cells with heptanoate (C7, a product of triheptanoin metabolism) corrects all aspects of the signalling defect and restores sensitivity to metabolic stress to control levels. The underlying mechanism is that heptanoate is converted to acetyl CoA and propionyl CoA, both of which enter and help boost the TCA cycle and correct the mitochondrial function in ATM-deficient cells. More functional mitochondria lead to enhanced interaction with the ER which increases the transfer of Ca^{2+} to promote cell survival. These results suggest that heptanoate by increasing access to TCA intermediates improves mitochondrial efficiency and in turn improves ER-mitochondrial interaction and cell bioenergetics. The TCA cycle depicted here is a simpler version involving some of the key metabolites and is not comprehensive.

ion homeostasis genes in these cells (Lai J, 2021). Hence, the capacity of the triheptanoin metabolite heptanoate to correct all aspects of mitochondrial function and signalling supports this approach to therapeutic intervention in A-T patients.

AUTHOR CONTRIBUTION

All authors made substantial contributions to the research. MFL, AJY, and DC were involved in the conception and design of the work. Experimental procedures were performed by AJY, GNS, KLC, MG, and RP. Analysis and interpretation of data were carried out by MFL, AJY, DC, and GNS. The manuscript was drafted by MFL, AJY, and GNS and critically reviewed by all authors. All authors also approved the final version submitted.

ETHICS DECLARATION

Sample collections for patient airway epithelial cells and all experimental procedures were performed in accordance with the guidelines provided in the NHMRC National Statement on Ethical Conduct in Human Research and Australian Code for the Responsible Conduct of Research after obtaining approval from the University of Queensland Human Research Ethics Committee (UQ HREC).

ACKNOWLEDGMENTS

This research work was funded by the BrAshA-T Foundation, Australia, The Children's Hospital, Foundation Australia (RM2018002270 to AJY, Wesley Medical Research Fund (Grant Ref. No. 2020—28), and The National Health and Medical Research Council Medical Research Future Fund, Australia (Grant Ref. No. APP1200255). RGP was supported by the National Health and Medical Research Council of Australia (Grant Ref. No. APP1140064 and APP1150083 and fellowship). We would like to acknowledge the staff at Metabolomics Australia (Queensland) at Australian Institute for Bioengineering and Nanotechnology (AIBN) for helping with the LC-MS analysis and data processing pertaining to metabolomic analysis and Charles Ferguson (IMB) for processing cells for electron microscopy. The authors acknowledge the help of staff and use of facilities in the Microscopy Australia NCRIS Facility at the Centre for Microscopy and Microanalysis at The University of Queensland. We would also like to acknowledge Professor Peter Sly and Sally Galbraith at Children's Health and Environment Program, UQ Child Health Research Centre (CHRC) for collecting nasal scrapings from A-T patients and controls. We would also like to acknowledge A-T patients and their families for their kind support.

CONFLICT OF INTEREST

The authors declare no competing interests pertinent to this study.

APPENDIX A. SUPPLEMENTARY DATA

Supplementary data to this article can be found online at https://doi.org/10.1016/j.molmet.2021.101354.

REFERENCES

[1] Lavin, M.F., 2008. Ataxia-telangiectasia: from a rare disorder to a paradigm for cell signalling and cancer. Nature Reviews Molecular Cell Biology 9(10):759–769.

[2] McKinnon, P.J., 2012. ATM and the molecular pathogenesis of ataxia telangiectasia. Annual Review of Pathology: Mechanisms of Disease 7:303–321.

[3] Mirzoeva, O.K., Petrini, J.H., 2003. DNA replication-dependent nuclear dynamics of the Mre11 complex. Molecular Cancer Research 1(3):207–218.

[4] Uziel, T., et al., 2003. Requirement of the MRN complex for ATM activation by DNA damage. The EMBO Journal 22(20):5612–5621.

[5] Bakkenist, C.J., Kastan, M.B., 2003. DNA damage activates ATM through intermolecular autophosphorylation and dimer dissociation. Nature 421(6922):499–506.

[6] Kozlov, S.V., et al., 2006. Involvement of novel autophosphorylation sites in ATM activation. The EMBO Journal 25(15):3504–3514.

[7] Kozlov, S.V., et al., 2011. Autophosphorylation and ATM activation: additional sites add to the complexity. Journal of Biological Chemistry 286(11):9107–9119.

[8] Shiloh, Y., Ziv, Y., 2013. The ATM protein kinase: regulating the cellular response to genotoxic stress, and more. Nature Reviews Molecular Cell Biology 14(4):197–210.

[9] Valentin-Vega, Y.A., et al., 2012. Mitochondrial dysfunction in ataxia-telangiectasia. Blood 119(6):1490–1500.

[10] Guo, Z., et al., 2010. ATM activation by oxidative stress. Science 330(6003):517–521.

[11] Paull, T.T., 2015. Mechanisms of ATM activation. Annual Review of Biochemistry 84:711–738.

[12] Yeo, A.J., et al., 2017. Loss of ATM in airway epithelial cells is Associated with Susceptibility to oxidative stress. American Journal of Respiratory and Critical Care Medicine 196(3):391–393.

[13] Yeo, A.J., et al., 2019. Increased susceptibility of airway epithelial cells from ataxia-telangiectasia to S. pneumoniae infection due to oxidative damage and impaired innate immunity. Scientific Reports 9(1):2627.

[14] Kamsler, A., et al., 2001. Increased oxidative stress in ataxia telangiectasia evidenced by alterations in redox state of brains from Atm-deficient mice. Cancer Research 61(5):1849–1854.

[15] Chen, P., et al., 2003. Oxidative stress is responsible for deficient survival and dendritogenesis in Purkinje neurons from ataxia-telangiectasia mutated mutant mice. Journal of Neuroscience 23(36):11453–11460.

[16] Shackelford, R.E., et al., 2004. Iron chelators increase the resistance of Ataxia telangeictasia cells to oxidative stress. DNA Repair 3(10):1263–1272.

[17] Reliene, R., Schiestl, R.H., 2006. Antioxidant N-acetyl cysteine reduces incidence and multiplicity of lymphoma in Atm deficient mice. DNA Repair 5(7):852–859.

[18] Blignaut, M., et al., 2019. Ataxia-Telangiectasia Mutated is located in cardiac mitochondria and impacts oxidative phosphorylation. Science Reports 9(1):4782.

[19] Watters, D., et al., 1997. Cellular localisation of the ataxia-telangiectasia (ATM) gene product and discrimination between mutated and normal forms. Oncogene 14(16):1911–1921.

[20] Zhang, J., et al., 2015. ATM functions at the peroxisome to induce pexophagy in response to ROS. Nature Cell Biology 17(10):1259–1269.

[21] Lee, J.H., Paull, T.T., 2020. Mitochondria at the crossroads of ATM-mediated stress signaling and regulation of reactive oxygen species. Redox Biol 32:101511.

[22] Ambrose, M., Goldstine, J.V., Gatti, R.A., 2007. Intrinsic mitochondrial dysfunction in ATM-deficient lymphoblastoid cells. Human Molecular Genetics 16(18):2154–2164.

[23] Eaton, J.S., et al., 2007. Ataxia-telangiectasia mutated kinase regulates ribonucleotide reductase and mitochondrial homeostasis. Journal of Clinical Investigation 117(9):2723–2734.

[24] Fang, E.F., et al., 2016. NAD(+) replenishment improves Lifespan and Healthspan in ataxia telangiectasia Models via Mitophagy and DNA repair. Cell Metabolism 24(4):566–581.

[25] Chow, H.M., et al., 2019. ATM is activated by ATP depletion and modulates mitochondrial function through NRF1. The Journal of Cell Biology 218(3):909–928.

[26] Yeo, A.J., et al., 2021. Impaired endoplasmic reticulum-mitochondrial signaling in ataxia-telangiectasia. iScience 24(1):101972.

[27] Wehbe, Z., Tucci, S., 2020. Therapeutic potential of triheptanoin in metabolic and neurodegenerative diseases. Journal of Inherited Metabolic Disease 43(3):385–391.

[28] Shirley, M., 2020. Triheptanoin: first approval. Drugs 80(15):1595–1600.

[29] Gu, L., et al., 2010. Parenteral and enteral metabolism of anaplerotic triheptanoin in normal rats. II. Effects on lipolysis, glucose production, and liver acyl-CoA profile. American Journal of Physiology - Endocrinology And Metabolism 298(2):E362–E371.

[30] Yuan, X., et al., 2020. Triheptanoin mitigates brain ATP depletion and mitochondrial dysfunction in a mouse model of Alzheimer's disease. J Alzheimers Disease 78(1):425–437.

[31] Medina-Torres, C.E., et al., 2015. A liquid chromatography–tandem mass spectrometry-based investigation of the lamellar interstitial metabolome in healthy horses and during experimental laminitis induction. The Veterinary Journal 206(2):161–169.

[32] McDonald, T.S., et al., 2017. Alterations in Cytosolic and mitochondrial [U-^{13}C] glucose metabolism in a Chronic epilepsy mouse model. Eneuro 4(1) p. ENEURO.0341-16.2017.

[33] Dietmair, S., et al., 2012. A multi-omics Analysis of recombinant protein Production in Hek293 cells. PLoS One 7(8):e43394.

[34] Espinosa, M.I., et al., 2020. Adaptive laboratory evolution of native methanol assimilation in Saccharomyces cerevisiae. Nature Communications 11(1):5564.

[35] Zhang, Y., et al., 2018. Mitochondrial redox sensing by the kinase ATM maintains cellular antioxidant capacity. Science Signaling 11(538).

[36] Kim, J., Wong, P.K., 2009. Oxidative stress is linked to ERK1/2-p16 signaling-mediated growth defect in ATM-deficient astrocytes. Journal of Biological Chemistry 284(21):14396–14404.

[37] Gueven, N., et al., 2006. Dramatic extension of tumor latency and correction of neurobehavioral phenotype in Atm-mutant mice with a nitroxide antioxidant. Free Radical Biology and Medicine 41(6):992–1000.

[38] Csordás, G., et al., 2010. Imaging interorganelle contacts and local calcium dynamics at the ER-mitochondrial interface. Molecular Cell 39(1):121–132.

[39] Kornmann, B., et al., 2009. An ER-mitochondria tethering complex Revealed by a synthetic Biology screen. Science 325(5939):477.

[40] Gomez-Suaga, P., et al., 2017. The ER-mitochondria tethering complex VAPB-PTPIP51 regulates autophagy. Current Biology 27(3):371–385.

[41] Gomez-Suaga, P., et al., 2019. The VAPB-PTPIP51 endoplasmic reticulum-mitochondria tethering proteins are present in neuronal synapses and regulate synaptic activity. Acta Neuropathologica Communication 7(1):35.

[42] Yuan, L., et al., 2000. The murine SCP3 gene is required for synaptonemal complex assembly, chromosome synapsis, and male fertility. Molecular Cell 5(1):73–83.

[43] Phillips, M.J., Voeltz, G.K., 2016. Structure and function of ER membrane contact sites with other organelles. Nature Reviews Molecular Cell Biology 17(2):69—82.
[44] Pallafacchina, G., Zanin, S., Rizzuto, R., 2018. Recent advances in the molecular mechanism of mitochondrial calcium uptake. F1000Research 7.
[45] Qi, Y., et al., 2016. ATM mediates spermidine-induced mitophagy via PINK1 and Parkin regulation in human fibroblasts. Scientific Reports 6:24700.
[46] Kang, H.T., et al., 2017. Chemical screening identifies ATM as a target for alleviating senescence. Nature Chemical Biology 13(6):616—623.
[47] Xi, H., et al., 2011. 2-Deoxy-D-glucose activates autophagy via endoplasmic reticulum stress rather than ATP depletion. Cancer Chemotherapy and Pharmacology 67(4):899—910.
[48] Kobayashi, H., et al., 2015. Identification of the determinants of 2-deoxyglucose sensitivity in cancer cells by shRNA library screening. Biochemical and Biophysical Research Communications 467(1):121—127.
[49] Xu, L., et al., 2019. ATM deficiency promotes progression of CRPC by enhancing Warburg effect. Endocrine-Related Cancer 26(1):59—71.
[50] Chen, Q., et al., 2020. BRCA1 deficiency impairs Mitophagy and promotes inflammasome Activation and mammary tumor metastasis. Advancement of Science 7(6):1903616.
[51] Glancy, B., Balaban, R.S., 2021. Energy metabolism design of the striated muscle cell. Physiological Reviews 101(4):1561—1607.
[52] Glancy, B., et al., 2021. Mitochondrial lactate metabolism: history and implications for exercise and disease. The Journal of Physiology 599(3):863—888.
[53] Ždralević, M., et al., 2018. Double genetic disruption of lactate dehydrogenases A and B is required to ablate the "Warburg effect" restricting tumor growth to oxidative metabolism. Journal of Biological Chemistry 293(41):15947—15961.
[54] Dai, C., et al., 2020. Lactate dehydrogenase A governs cardiac hypertrophic Growth in Response to hemodynamic stress. Cell Reports 32(9):108087.
[55] McGrath-Morrow, S.A., et al., 2010. Evaluation and management of pulmonary disease in ataxia-telangiectasia. Pediatric Pulmonology 45(9):847—859.
[56] Rothblum-Oviatt, C., et al., 2016. Ataxia telangiectasia: a review. Orphanet Journal of Rare Diseases 11(1):159.
[57] Amirifar, P., et al., 2020. Ataxia-telangiectasia: epidemiology, pathogenesis, clinical phenotype, diagnosis, prognosis and management. Expert Review of Clinical Immunology 16(9):859—871.
[58] Schlam-Babayov, S., et al., 2021. Phosphoproteomics reveals novel modes of function and inter-relationships among PIKKs in response to genotoxic stress. The EMBO Journal 40(2):e104400.
[59] Balmus, G., et al., 2019. ATM orchestrates the DNA-damage response to counter toxic non-homologous end-joining at broken replication forks. Nature Communications 10(1):87.
[60] Bar, R.S., et al., 1978. Extreme insulin resistance in ataxia telangiectasia: defect in affinity of insulin receptors. New England Journal of Medicine 298(21):1164—1171.
[61] Schneider, J.G., et al., 2006. ATM-dependent suppression of stress signaling reduces vascular disease in metabolic syndrome. Cell Metabolism 4(5):377—389.
[62] Guleria, A., Chandna, S., 2016. ATM kinase: Much more than a DNA damage responsive protein. DNA Repair 39:1—20.
[63] Guo, Q.Q., et al., 2020. ATM-CHK2-Beclin 1 axis promotes autophagy to maintain ROS homeostasis under oxidative stress. The EMBO Journal 39(10): e103111.
[64] Wingard, M.C., et al., 2020. Heart failure and diabetes: role of ATM. Current Opinion in Pharmacology 54:27—35.
[65] Cirotti, C., et al., 2020. Redox activation of ATM enhances GSNOR translation to sustain mitophagy and tolerance to oxidative stress. EMBO Reports, e50500.
[66] D'Souza, A.D., et al., 2013. Reducing mitochondrial ROS improves disease-related pathology in a mouse model of ataxia-telangiectasia. Molecular Therapy 21(1):42—48.
[67] Shiloh, Y., Tabor, E., Becker, Y., 1982. Cellular hypersensitivity to neocarzinostatin in ataxia-telangiectasia skin fibroblasts. Cancer Research 42(6): 2247—2249.
[68] Taylor, A.M., et al., 1975. Ataxia telangiectasia: a human mutation with abnormal radiation sensitivity. Nature 258(5534):427—429.
[69] Chen, P.C., et al., 1978. Identification of ataxia telangiectasia heterozygotes, a cancer prone population. Nature 274(5670):484—486.
[70] Rossi, A., Pizzo, P., Filadi, R., 2019. Calcium, mitochondria and cell metabolism: a functional triangle in bioenergetics. Biochimica et Biophysica Acta (BBA) - Molecular Cell Research 1866(7):1068—1078.
[71] Szabadkai, G., et al., 2006. Chaperone-mediated coupling of endoplasmic reticulum and mitochondrial Ca2+ channels. The Journal of Cell Biology 175(6):901—911.
[72] Honrath, B., et al., 2017. Glucose-regulated protein 75 determines ER-mitochondrial coupling and sensitivity to oxidative stress in neuronal cells. Cell Death Discovery 3:17076.
[73] Rizzuto, R., et al., 2009. Ca(2+) transfer from the ER to mitochondria: when, how and why. Biochimica et Biophysica Acta 1787(11):1342—1351.
[74] Jones, A.W., Szabadkai, G., 2010. Ca(2)(+) transfer from the ER to mitochondria: channeling cell death by a tumor suppressor. Developmental Cell 19(6):789—790.
[75] Cardenas, C., et al., 2010. Essential regulation of cell bioenergetics by constitutive InsP3 receptor Ca2+ transfer to mitochondria. Cell 142(2):270—283.
[76] Steward, R., et al., 2013. A patient-derived olfactory stem cell disease model for ataxia-telangiectasia. Human Molecular Genetics 22(12):2495—2509.

